Maximum-entropy network analysis reveals a role for tumor necrosis factor in peripheral nerve development and function

Prabhjot S. Dhadialla[a], Ifije E. Ohiorhenuan[b], Andrew Cohen[a], and Sidney Strickland[a,1]

[a]Laboratory of Neurobiology and Genetics, The Rockefeller University, New York, NY 10065; and [b]Department of Neurology, Weill Cornell New York Hospital, New York, NY 10065

Edited by Anthony Cerami, Warren Pharmaceuticals, Inc., Ossining, NY, and approved May 4, 2009 (received for review February 27, 2009)

Gene regulatory interactions that shape developmental processes can often can be inferred from microarray analysis of gene expression, but most computational methods used require extensive datasets that can be difficult to generate. Here, we show that maximum-entropy network analysis allows extraction of genetic interactions from limited microarray datasets. Maximum-entropy networks indicated that the inflammatory cytokine TNF-α plays a pivotal role in Schwann cell–axon interactions, and these data suggested that TNF mediates its effects by orchestrating cytoplasmic movement and axon guidance. In vivo and in vitro experiments confirmed these predictions, showing that Schwann cells in TNF$^{-/-}$ peripheral sensory bundles fail to envelop axons efficiently, and that recombinant TNF can partially correct these defects. These data demonstrate the power of maximum-entropy network-based methods for analysis of microarray data, and they indicate that TNF-α plays a direct role in Schwann cell–axon communication.

As the density of genetic regulatory information increases, so does the importance of identifying pivotal molecules that regulate complex processes. Perturbation of these molecules provides insight into the relationship between development processes and therapeutic possibilities. Although a variety of techniques are used to categorize genes transcription profiles in order to determine aggregate patterns, most provide little insight into inferred gene network interactions (1-3). Undersampled datasets perform poorly under the model-constraining assumptions in linear models such as Bayesian or relevance networks (4, 5). Maximum-entropy networks are used to successfully represent complex interactions in diverse nonequilibrium systems, including genetic and neural networks based on pairwise interactions (6, 7). This method is predicated upon constructing a network topology from pairwise interactions that uses a modified maximum-entropy approach to empirically explain the resulting transcriptional profile. Previous studies of maximum-entropy networks to represent genetic transcriptional information confirm the utility of the approach and suggest hypotheses for further experimental exploration (6, 8, 9).

We have adapted this method to analyze the genetic network of peripheral nerve development by using dorsal root ganglia (DRG) cocultures, followed by a rapid screen for motor or sensory dysfunction using available transgenic mice. This was followed by in vivo sciatic nerve assessment, and in vitro studies in the DRG coculture system (Fig. 1). Studies have shown that genetic networks contain network hubs, where relationships between genes and the number of linkages between is logarithmic (8, 10). The network hubs we identified were enriched with genes encoding proteins known to play a role in the nervous and immune systems, including TNF. This target list was unique to the modified maximum-entropy approach and indicated that the inflammatory cytokine TNF-α plays a pivotal role in Schwann cell–axon interactions. Local network information suggested that TNF mediates its effects by orchestrating cytoplasmic movement and axon guidance. Patients receiving anti-TNF therapy experience nervous system pathologies (11). Although this has been largely attributed to the sequelae of an immune response, an alternative hypothesis is that nervous system tissues that use these molecules for communication are disrupted (12, 13). Indeed, these hypotheses are not mutually exclusive.

Based on the first-degree network of TNF, we speculated that TNF could play a role in axonal guidance and cytoplasmic extension. Studies of TNF localized in Schwann cell cytoplasm (14) and expressed in an autocrine and local paracrine fashion (15) have shown that TNF can directly modulate synaptic scaling in the spinal cord (16). We reported that TNF$^{-/-}$ transgenic mice experienced sensory latency and had impaired Schwann cell to multiaxon interactions in in vivo and in vitro DRG coculture systems. We showed that anti-TNF antibody can induce similar dysfunction in wild-type cocultures, leading to a concomitant disruption of Netrin-1 and TNF receptor 1 localizations. Finally, we showed that impaired Schwann cell–axonal interactions can be partially restored with recombinant TNF (rTNF). These data demonstrate the utility of maximum-entropy network-based methods for analysis of microarray data and indicate that modulation of the TNF-α pathway may serve a therapeutic role in peripheral nerve sensory disorders.

Results

Entropy-Maximized Network Structure of DRG Coculture Microarray Is Stable. Microarray studies of peripheral nerve development have used in vivo sciatic nerve tissue to cluster genes with similar transcriptional profiles (17, 18). We used the DRG coculture system because the addition of ascorbic acid triggers the maturation of Schwann cell and neuronal interactions (19)—allowing finer temporal sampling than previously achieved—at 0, 0.5, 1, 6, 12, 24, 36, 48 h after addition of ascorbic acid (Fig. 1*A*).

The analysis approach we followed represents an integration of traditional prioritization of variance by transcriptional levels coupled with pairwise comparison of these profiles to determine a covariance score. The covariance score creates a cutoff for linkage that can be used to construct a network map. After choosing the 500 most variant transcriptional profiles (≈2- to 3-fold changes from baseline), we constructed individual interaction profiles of each gene with all others in the network to determine an appropriate covariance cutoff score (Fig. S1). We visualized the resulting pairwise interaction network when the cutoff score was defined as 2 or 3 SDs from a covariance score of 0 for individual interaction profiles, and we found that 148 and 70 genes, respectively, were included as nodes in the resulting map (Fig. 1*B*). We determined whether this network is representative of previously described genetic network structures by analyzing how many links each node

Author contributions: P.S.D. and I.E.O. designed research; P.S.D., I.E.O., and A.C. performed research; P.S.D., I.E.O., and S.S. analyzed data; and P.S.D., I.E.O., and S.S. wrote the paper.

The authors declare no conflict of interest.

This article is a PNAS Direct Submission.

Data deposition: The data reported in this paper have been deposited in the Gene Expression Omnibus (GEO) database, www.ncbi.nlm.nih.gov/geo, MIAME compatible (accession no. GSE16729).

[1]To whom correspondence should be addressed. E-mail: strickland@rockefeller.edu.

This article contains supporting information online at www.pnas.org/cgi/content/full/0902237106/DCSupplemental.

www.pnas.org/cgi/doi/10.1073/pnas.0902237106

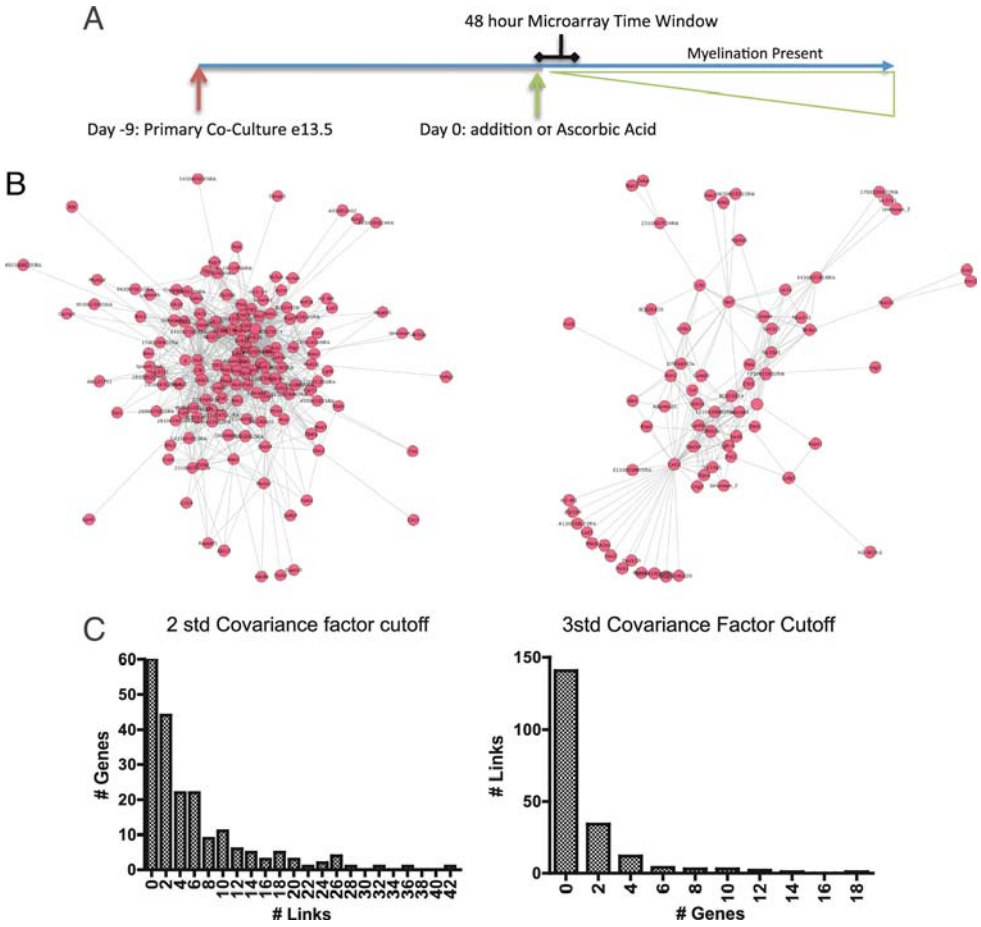

Fig. 1. Entropy-maximized network structure of DRG coculture microarray. (*A*) Triplicate samples of wild-type DRG cocultures were obtained at 0, 0.5, 1, 6, 12, 24, 36, and 48 h after the addition of ascorbic acid. (*B*) Visualization of the resulting entropy-maximized network with 2 and 3 SD covariance factor cutoffs, with 148 and 70 genes included, respectively. (*C*) For the 2 and 3 SD cutoffs, the number of links was plotted against the number of genes in the network as a histogram, indicating that a few genes have the most network interconnections.

had, and found it to be consistent (Fig. 1*C*) (8, 10, 20). The nodes with the greatest number of links were consistent if the covariance cutoff score was set at 2 or 3 SDs, indicating that the network structure was stable (Table S1). The DRG coculture network hubs include *netrin-1*, *Chemokine* (C-X-C motif) ligand 2, EDAR-associated death domain, and TNF, members of the NF-κB transcriptional network (21–24), which is involved in neurite outgrowth, axon insulation, and the activation of Schwann cells (25, 26). These data indicated that the network analysis approach yields groups of functionally related genes and some with known function in peripheral nerve development.

TNF Is a Network Hub in Peripheral Nerve Development That Links Cellular Processes. TNF emerged as a highly linked node as the covariance cutoff stringency increased (Table S1). In comparison, TNF appeared as 179th of 200 genes in conventional variance analysis (Table S2), making it unlikely that it would have been a priority for further exploration. Previous studies have shown that TNF is involved in the activation of Schwann cells, long-term potentiation of sensory nerve fibers after injury, and the development of neuropathic pain (27–29). We isolated the first-degree neighbors of TNF in the model network and explored the literature for known interactions with TNF or TNF-related signaling networks (Fig. S2). Of the 11 genes in the local TNF network, 2 major groups of genes with related signaling components emerged on an axis of decreasing connectedness to other local TNF network genes. The group with a greater degree of network connectedness with TNF was related to NF-κB, which has a well characterized role in the transcriptional regulation of peripheral nerve development. This group included netrin-1, which plays a role in axon guidance. The second group included genes related to networks involved in cytoplasmic extension, enervation, and Schwann cell function (Table S3) (30–35). TNF is more tightly connected with the first group at the more fundamental level of transcriptional control related to NF-κB, compared with the cellular effectors represented in the second group, suggesting that TNF is a network node that intersects with these 2 groups. These results suggested that we should investigate the relevance of TNF in peripheral nerve function.

TNF$^{-/-}$ Mice Experience Sensory Latency to Thermally Painful Stimuli. To assess the role of TNF in peripheral nerve function, we sought to determine whether TNF$^{-/-}$ mice had any phenotypic neurological defects. The rotarod test integrates motor and proprioceptive aspects of peripheral nerve function. There were no significant differences in performance (Fig. 2*A*). Studies indicated that anti-

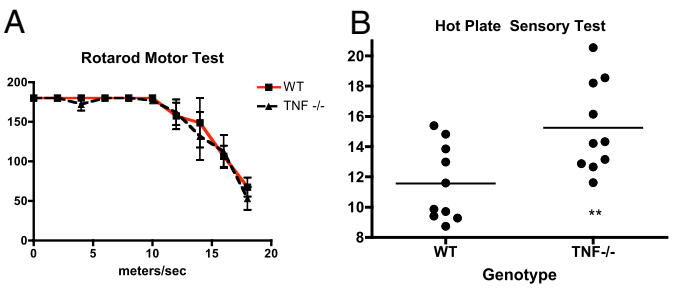

Fig. 2. TNF$^{-/-}$ mice showed increased paw withdrawal latency by hot plate test. (*A*) There was no significant difference between the rotarod performance of wild-type and TNF$^{-/-}$ mice. (*B*) TNF$^{-/-}$ mice had significantly increased paw withdrawal latency compared with wild-type mice by using the hot plate test ($P = 0.0093$).

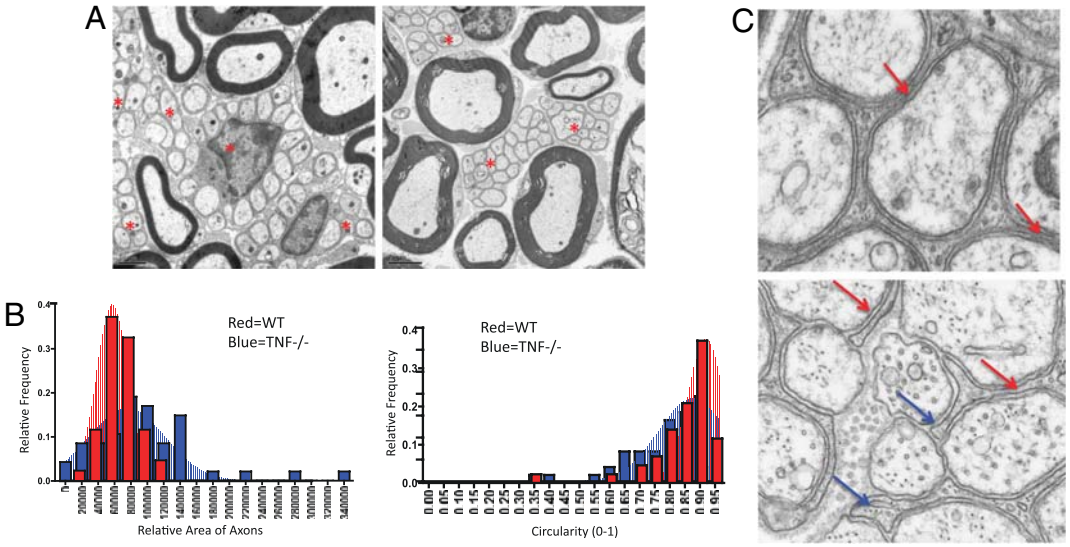

Fig. 3. TNF$^{-/-}$ mice had significant variation in the area of axons within sciatic nerve Remak/sensory bundles. (*A*) Electron micrographs of Remak bundles (*) suggested differences in the circularity and size variation of axons in wild-type vs. TNF$^{-/-}$ mouse sciatic nerves. (*B*) The relative variation of area of axons in wild-type vs. TNF$^{-/-}$ Remak sensory bundles was significant ($P < 0.0001$), with more outliers in axonal size in TNF$^{-/-}$ sciatic nerves. The variation in Remak axon circularity did not meet significance ($P = 0.7534$). (*C*) Examination of Remak bundle Schwann cell–axon relationships revealed greater spaces between TNF$^{-/-}$ Schwann cells and axons (red arrows), as well as incomplete Schwann cell cytoplasmic envelopment of axons (blue arrows), resulting in adjacent, uninsulated axons.

TNF neutralizing antibody reduces peripheral nerve sensory function in pain models as well as in normal patients (27, 28, 36–38), potentially through ion channels in nociceptive neurons (13). We directly assessed sensory function in response to thermal stimuli by using the hot plate test. Wild-type mice withdraw their paws significantly faster than TNF$^{-/-}$ mice ($P = 0.0082$), indicating that TNF$^{-/-}$ mice experience sensory latency (Fig. 2*B*). This defect in the TNF$^{-/-}$ mice suggests an abnormality in the Remak bundles that contain unmyelinated axons that carry sensory information.

TNF$^{-/-}$ Mice Have Abnormal Axon Size Variation in Remak Sensory Bundles. To explore the basis of the sensory latency in TNF$^{-/-}$ mice, we compared the Remak bundles in sciatic nerve cross-sections of 21-day-old wild-type and TNF$^{-/-}$ mice. Remak sensory bundles convey pain information through the interaction of individual Schwann cells and multiple axons. Compared with wild-type mice, the Remak bundles of TNF$^{-/-}$ mice appeared to have greater axonal size variation. We analyzed the images by using ImageJ software (National Institutes of Health) to quantitate this differ-

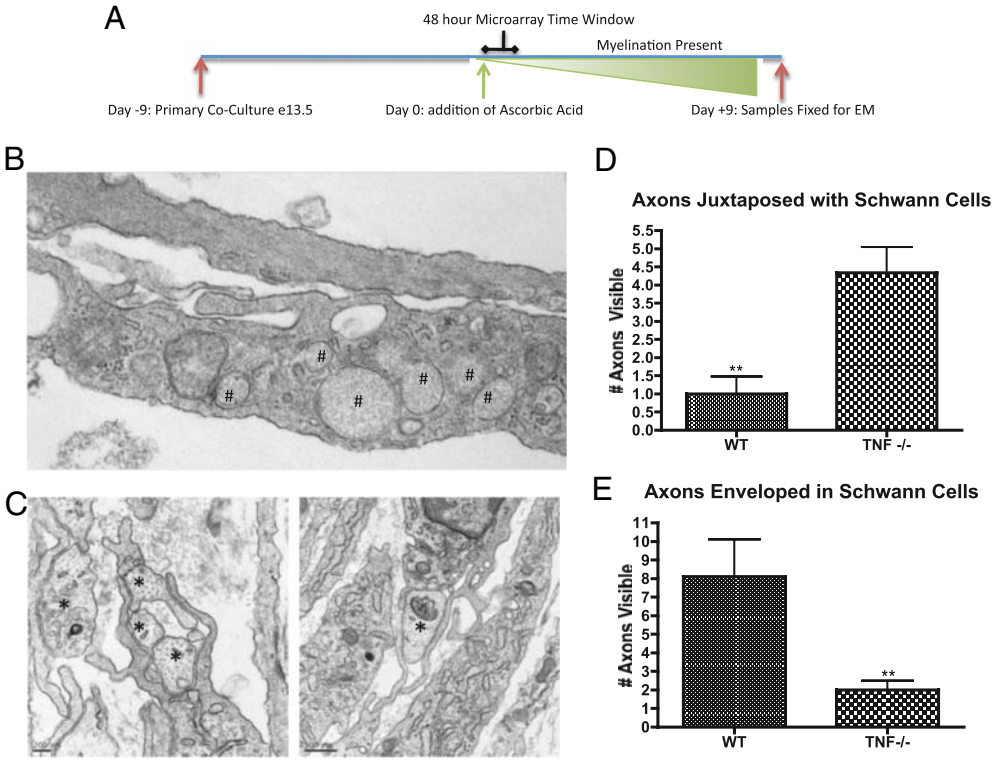

Fig. 4. TNF$^{-/-}$ nonmyelinating Schwann cells did not efficiently envelope axons. (*A*) Timeline for fixation of coculture samples in preparation for EM, allowing time for the maturation of myelinating Schwann cell–axon interactions. (*B*) Wild-type Schwann cells enveloped multiple axons into their cytoplasm (#), which had a uniformly round appearance. (*C*) TNF$^{-/-}$ Schwann cells extended long cytoplasmic processes in search of axons while bypassing potential productive interactions (*). (*D*) The number of axons directly juxtaposed with Schwann cells was significantly higher in TNF$^{-/-}$ cocultures ($n = 9$; $P = 0.0012$). (*E*) The number of axons enveloped by the same Schwann cell (as quantified in *D*) cytoplasm was significantly higher in wild-type cocultures ($n = 9$; $P = 0.009$; **, $P < 0.01$.

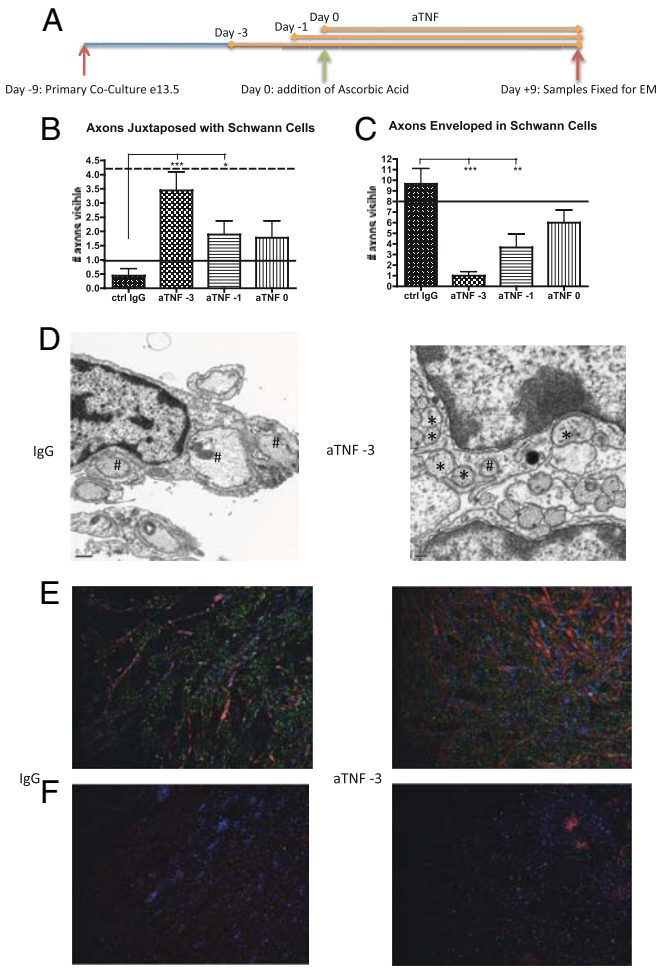

Fig. 5. TNF-blocking antibody administration (aTNF) in wild-type DRG cocultures resulted in decreased Schwann cell–axon envelopment. (*A*) The aTNF and control IgG were added at day −3, aTNF at day −1 and day 0 until samples fixed for EM at day +9. (*B*) The number of axons juxtaposed with Schwann cells was significantly increased when aTNF was administrated at day −3 compared with control antibody (3.44 vs. 0.44; $n = 9$; $P = 0.005$). (*C*) The number of axons enveloped by Schwann cells was significantly decreased when aTNF was administrated at day −3 compared with control antibody (1.00 vs. 9.67; $n = 9$; $P < 0.0001$). (*D*) Electron micrograph of control antibody and TNF-blocking antibody treatment at day −3 showed an increase in axons juxtaposed to Schwann cells (*) with TNF-blocking antibody treatment (*). (*E*) Immunofluorescence of cocultures with control IgG and TNF-blocking antibody of neurons (red), Schwann cells (blue), and TNF (green). Schwann cells and neurons colocalized with control antibody administration, compared with separation evident with TNF-blocking antibody, and TNF expression is localized vs. diffuse. (*F*) Netrin-1 (blue) was clustered and TNFR1 was diffuse in the presence of control antibody, whereas this relationship was switched in the presence of TNF-blocking antibody.

ence, and we found significantly that in $TNF^{-/-}$ Remak bundles, there was a greater variation in axonal size (F test, $P < 0.00001$) (Fig. 3*A*) but not in axon circularity (F test, $P < 0.07534$), which was done as a control for morphological defects that could arise during fixation and EM preparation (Fig. 3*B*). Closer examination of the Remak bundles revealed poor incorporation of axons in Schwann cell cytoplasm and incomplete ensheathment (Fig. 3*C*). These results suggested that TNF is involved in the process of axonal ensheathment by Schwann cell cytoplasm as well as modulation of axonal size, supporting previous molecular studies describing local interactions between Schwann cells and axons (39).

Nonmyelinating Schwann Cells in $TNF^{-/-}$ DRG Cocultures Do Not Efficiently Incorporate Axons. To investigate the relationship between Schwann cells and axons, we generated DRG cocultures from $TNF^{-/-}$ mice and wild-type mice for analysis by EM (Fig. 4*A*). Both $TNF^{-/-}$ and wild-type mature DRG cocultures contained myelinated axons and Schwann cells with multiaxon relationships. Schwann cells can myelinate 1 axon or envelop multiple nonmyelinated axons. These latter Schwann cells are characterized by the envelopment of multiple, circular axons with short cytoplasmic extensions at the leading edge in wild-type cocultures (Fig. 4*B*). In $TNF^{-/-}$ cocultures, multiple unmyelinated axons are juxtaposed with Schwann cells that have extensive cytoplasmic extensions rather than enveloped into the cytoplasm (Fig. 4*C*). The axons also appeared to be irregularly shaped, with wide size variation. The number of axons juxtaposed with and enveloped in the cytoplasm of nonmyelinating Schwann cells were assessed for significant difference. Wild-type Schwann cells had fewer axons juxtaposed with them compared with $TNF^{-/-}$ mice (1.0 vs. 4.3, $P = 0.0012$; $n = 9$) (Fig. 4*D*). These same wild-type Schwann cells had more axons enveloped in their cytoplasm than those in the $TNF^{-/-}$ coculture (8.1 vs. 2.0, $P = 0.009$; $n = 9$) (Fig. 4*E*). These results suggest that there was a decrease in functional interaction between nonmyelinating Schwann cells and axons in the absence of TNF.

The Administration of Anti-TNF Antibody Disrupts Nonmyelinating Schwann Cell–Axon Interactions. Studies have shown that blocking TNF receptors mediates a decrease in sensory function in models of thermal, mechanical, and neuropathic pain sensitization (12, 37, 38). We speculated that the mechanism of decreased pain is due to disruptions in Schwann cell–multiaxon interactions. We explored the effect of saturating quantities of TNF-blocking antibody for different durations (added at days −3, −1, and 0; IgG antibody was added on day −3) in the wild-type coculture system before the addition of ascorbic acid (time 0) according to the timeline shown in Fig. 5*A*. The number of axons juxtaposed with Schwann cells was significantly higher when TNF-blocking antibody was added at day −3 compared with control antibody (day −3, 3.44 vs. 0.44; $P = 0.0005$; $n = 9$) (Fig. 5*B*). Conversely, the number of axons enveloped by Schwann cells was significantly lower (day −3, 1.0 vs. 9.67; $P < 0.0001$; $n = 9$) (Fig. 5*C*).

Electron micrographs of nonmyelinating Schwann cell–axon interactions in the presence of IgG or anti-TNF antibody are shown in Fig. 5*D*, depicting the increase in juxtaposed axons and decrease in enveloped axons when the TNF pathway was disrupted. To understand the spatial localization of TNF in relation to Schwann cells and neurons, we performed immunofluorescence with IgG and TNF-blocking antibody (day −3) treatment. In the presence of a control antibody, Schwann cells and neurons overlapped, and TNF was found in localized plumes next to the cells. In contrast, Schwann cells and neurons did not overlap in the presence of TNF-blocking antibody, and TNF was present diffusely in relation to cells (Fig. 5*D*). The expression of netrin-1 and TNF receptor 1 is correlated to NF-κB transcription (40, 41). The localization of netrin-1 in relation to TNF and TNF receptor 1 was examined to determine the validity of a network-predicted relation. In the presence of a control antibody, netrin-1 was present in localized aggregates, whereas the TNF receptor 1 was relatively diffuse, and this relationship was inverted in the presence of TNF-blocking antibody (Fig. 5*E*). Together, these findings indicate that TNF signaling and netrin-1 might act in concert to mediate Schwann cell–axonal interactions is a valid assumption, along with the involvement of TNF receptor 1. These data suggested that the TNF signaling pathway is a necessary component of physiologic Schwann cell–axonal interactions and that it is specifically disrupted in the presence of TNF-blocking antibody.

rTNF Partially Restores Impaired Schwann Cell–Multiaxon Interactions in $TNF^{-/-}$ Cocultures. To determine whether impaired Schwann cell–multiaxon interactions in $TNF^{-/-}$ could be restored, we added rTNF in 10-fold dilution (5, 0.5, and 0.05 ng/mL) to cocultures at day −3 until fixation at day +9 (Fig. 6*A*). The

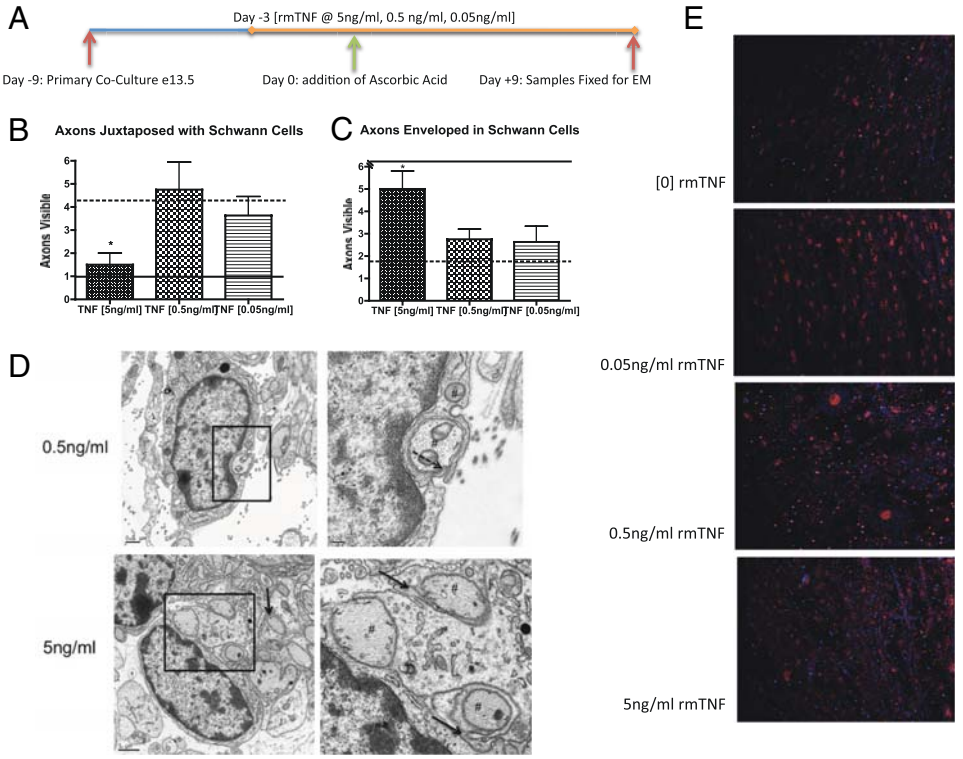

Fig. 6. The rTNF partially restored Schwann cell–axonal interactions in $TNF^{-/-}$ cocultures. (*A*) The rTNF was administered at day −3 at 5, 0.5, and 0.05 ng/mL. (*B*) The administration of 5 ng/mL rTNF resulted in significantly fewer juxtaposed axons to (*) Schwann cells compared with a 10-fold lower dose (1.50 vs. 4.75; $n = 9$; $P = 0.025$). (*C*) The administration of 5 ng/mL rTNF resulted in significantly more axons enveloped in (#) Schwann cell cytoplasm compared with a 10-fold lower dose (5.00 vs. 2.75; $n = 9$; $P = 0.028$). (*D*) Electron micrograph of Schwann cell–axonal interactions with 0.5 ng/mL or 5 ng/mL rTNF, with Schwann cell cytoplasmic extensions enveloping multiple axons (dashed black line) and encircling multiple axons (solid black arrows) depicted in the *Inset*. Panels on the *Right* are higher magnifications of the panels on the *Left*. (*E*) Increasing concentrations of rTNF partially disrupted TNFR1 clusters (red) and resulted in partial netrin-1 (blue) clustering. *, $P < 0.05$.

addition of 5 ng/mL rTNF resulted in significantly fewer axons juxtaposed with Schwann cells compared with 0.5 and 0.05 ng/mL ($P = 0.025$ and $P = 0.044$, respectively; $n = 9$) (Fig. 6*B*). Conversely, the addition of 5 ng/mL rTNF resulted in significantly more axons enveloped in Schwann cells compared with 0.5 ng/mL ($P = 0.028$; $n = 9$) (Fig. 6*C*). Electron micrographs of Schwann cell–axonal interactions with 0.5 ng/mL depicted Schwann cell cytoplasmic extensions enveloping an axon (Fig. 6*D Inset*, dashed black line) adjacent to a fully incorporated axon. With 5 ng/mL rTNF, the Schwann cell cytoplasm continued to encircle multiple axons (Fig. 6*D Inset*, solid black arrows) rather than fully incorporating it. Increasing concentrations of rTNF partially disrupted TNFR1 clusters (red) and resulted in partial netrin-1 (blue) clustering, indicating that rTNF administration does not fully restore $TNF^{-/-}$ cocultures to match wild-type markers (Fig. 6*E*). These data indicated that initial Schwann cell–axon interactions of recognition and envelopment are mediated by TNF and that further incorporation of axons into the Schwann cell cytoplasm was mediated by other factors.

Discussion

In this study, gene candidate predictions made employing maximum-entropy networks are experimentally confirmed to reveal functional information, suggesting that this a useful approach to understanding complex interactions using existing or new microaray data. Maximum-entropy analysis of microarray data differs from clustering because it moves beyond covariance to describe the interrelated structure of complex systems, such as gene networks. Previous microarray datasets used to explore the utility of maximum-entropy analysis in genetic networks have either been periodic, heavily sampled, or include transcriptional profiles that vary far greater than ≈2- to 3-fold (6); we were encouraged by the presence of genes with known or tangentially related function to nervous system development, function, or attendant cellular processes. In the in vitro DRG coculture model system, we showed that TNF is a predicted component of normal maturation of Schwann cell–neuronal interactions via maximum-entropy network analysis. The availability of transgenic mice and molecular tools made TNF an obvious choice for exploring the relationship between a cytokine in the context of endogenous peripheral nerve function. Further analysis of the first-degree TNF network implicated NF-κB transcriptional pathways as well as downstream cytoplasmic motor function, providing sufficient information to construct a hypothesis in concert with published literature.

We demonstrated that $TNF^{-/-}$ mice have increased latency to thermal stimuli and normal motor function, suggesting that there would be abnormalities in the Remak bundles of sciatic nerves. The spatial constraints of an organized tissue provide structural boundaries that can minimize the effects of dysfunctions that would be more apparent in cell culture. Through histologic and DRG coculture analysis of $TNF^{-/-}$ mice by electron microscopy, we demonstrated that Schwann cell–multiaxonal interactions were disrupted. These data suggest that TNF mediates communication between Schwann cells and axons in concert with associated signaling networks during peripheral nerve development. This is underscored by partial restoration of Schwann cell–axon interactions in $TNF^{-/-}$ cocultures in the presence of rTNF. The pursuit of TNF was also motivated by clinical studies of anti-TNF antibody treatment that implicate TNF's role in the nervous system as secondary to immune reactions, whereas experimental studies have shown that TNF is capable of acting as a primary effector of nervous system function. We found that administration of anti-TNF antibody in the in vitro DRG coculture system recapitulated the effects of the $TNF^{-/-}$ mice, suggesting that it is possible to induce impaired sensory function by modulating access to TNF signaling networks between nonmyelinating Schwann cells and axons.

These findings indicate that patients undergoing systemic administration of anti-TNF antibody should be carefully monitored for the management of neuropathies that emerge during the course of treatment. The availability of TNF neighborhood networks in conjunction with known signaling transduction pathways will facilitate the elucidation of relevant temporal and spatial molecular interactions.

The maximum-entropy network we describe to explore the role of TNF can be applied broadly to the richly available microarray

data of complex processes to provide an entry to understanding relevant molecular relationships. The network we describe in this study has been limited to the 500 most variant genes during the 48 h after the triggering of a maturation process between 2 dominantly represented cell types. As the time boundaries and experimental conditions change, variant network maps will emerge. If these variant networks are mapped in relation to each other, it will be possible to better understand the common molecular network features that underlie complex processes across tissues. In the meantime, screening of predicted gene candidates should be informed by the availability of resources, cost of exploration, and clinical relevance. We suggest that to exercise the utility of preexisting microarray data, entropy should be maximized as part of an orderly process.

Materials and Methods

DRG Coculture and Associated Reagents. Wild-type mice were obtained at embryonic day 13.5 for the extraction of DRG, which contain 2 main cell populations: Schwann cells and neurons. The DRG was disassociated and maintained until a dense layer of Schwann cells existed in tight proximity to neurons (−9 days). The onset of Schwann cell–axonal maturation was triggered by adding ascorbic acid, defining time point zero as described in ref. 42. Samples for microarray analysis were obtained in triplicate from separate coculture slips at 0, 0.5, 1, 6, 12, 36, and 48 h after ascorbic acid addition and were prepared for use on Illumina Mouse-8 chips (Illumina) by the Rockefeller Microarray Core Facility (New York, NY). Cocultures for EM analysis were obtained at day 9. The TNF-neutralizing antibody (Abcam) was administered to cocultures at saturating concentrations (reported $ND_{50} = 0.08–0.1$ μg/mL; 1 μg/mL used). A polyclonal IgG control (Abcam) was used at the same concentration. The rTNF (R&D Systems) was administered at 5, 0.5, and 0.05 ng/mL.

Network Analysis. For microarray data, the expression levels of genes at time t can be considered to be a vector, x, of n genes. Sampling gene expression levels at different times leads to a distribution over these vectors, which describes the behavior of the network. One simplification is to assume that the behavior of the network is determined completely by interactions between pairs of genes and not by any higher interactions (such as interactions between triplets). As shown by Lezon et al. (6), the matrix of interaction strengths M between genes is simply the inverse of the covariance matrix of the expression levels of these genes.

In our analysis, we normalized and then averaged the raw expression data by using Illumina software. Further analyses were performed by using custom software written in Matlab (MathWorks, Natick, MA). We selected only those genes that are reliably detected at all time points with a detection P value >0.9. Expression levels for each gene are rendered relative to baseline by subtracting out expression levels at time 0. We then select the n genes (typically 200–500) whose expression level has the highest variance over the course of the experiment. This forms an N-by-t array, X, of n genes, sampled at t times. We calculate the covariance matrix of this array C_{ij}, which describes the variance of each gene i with every other gene j. Because this matrix is generally noninvertible, we calculate the pseudoinverse, M_{ij}, which contains the interaction strengths for each gene i with every other gene j. To determine which genes have a significant interaction, we threshold the interaction strengths: interactions that are 2 or 3 SDs above (or below) the mean are counted as positive (or negative) interactions. The network was visualized by using Cytoscape software (National Institutes of Health) using spring-embedded and degree-weighted views without considering the directionality of interactions. This approach is considered a ''modified maximum-entropy'' approach because the dataset is first filtered by variance to limit the scope of calculation.

ACKNOWLEDGMENTS. This work was supported by National Institutes of Health Grant NS038472; the Dr. Miriam and Sheldon G. Adelson Medical Research Foundation; the Paul and Daisy Soros Fellowship (to P.S.D.); and Medical Scientist Training Program Grant GM07739 (to P.S.D. and I.E.O.).

1. Pan W (2002) A comparative review of statistical methods for discovering differentially expressed genes in replicated microarray experiments. *Bioinformatics* 18:546–554.
2. D'Haeseleer P (2005) How does gene expression clustering work? *Nat Biotechnol* 23:1499–1501.
3. D'Haeseleer P, Liang S, Somogyi R (2000) Genetic network inference: From co-expression clustering to reverse engineering. *Bioinformatics* 16:707–726.
4. Tegner J, Yeung MK, Hasty J, Collins JJ (2003) Reverse engineering gene networks: Integrating genetic perturbations with dynamical modeling. *Proc Natl Acad Sci USA* 100:5944–5949.
5. Li S, Wu L, Zhang Z (2006) Constructing biological networks through combined literature mining and microarray analysis: A LMMA approach. *Bioinformatics* 22:2143–2150.
6. Lezon TR, Banavar JR, Cieplak M, Maritan A, Fedoroff NV (2006) Using the principle of entropy maximization to infer genetic interaction networks from gene expression patterns. *Proc Natl Acad Sci USA* 103:19033–19038.
7. Schneidman E, Berry MJ, 2nd, Segev R, Bialek W (2006) Weak pairwise correlations imply strongly correlated network states in a neural population. *Nature* 440:1007–1012.
8. Fernandez A (2007) A molecular basis for evolving modularity in the yeast protein interaction network. *PLoS Comput Biol* 3:e226.
9. Manke T, Demetrius L, Vingron M (2006) An entropic characterization of protein interaction networks and cellular robustness. *J R Soc Interface* 3:843–850.
10. Ravasz E, Somera AL, Mongru DA, Oltvai ZN, Barabasi AL (2002) Hierarchical organization of modularity in metabolic networks. *Science* 297:1551–1555.
11. Stubgen JP (2008) Tumor necrosis factor-alpha antagonists and neuropathy. *Muscle Nerve* 37:281–292.
12. Empl M, et al. (2001) TNF-alpha expression in painful and nonpainful neuropathies. *Neurology* 56:1371–1377.
13. Czeschik JC, Hagenacker T, Schafers M, Busselberg D (2008) TNF-alpha differentially modulates ion channels of nociceptive neurons. *Neurosci Lett* 434:293–298.
14. Cheng C, et al. (2007) Induction of TNF-alpha by LPS in Schwann cell is regulated by MAPK activation signals. *Cell Mol Neurobiol* 27:909–921.
15. Qin Y, et al. (2008) TNF-alpha as an autocrine mediator and its role in the activation of Schwann cells. *Neurochem Res* 33:1077–1084.
16. Stellwagen D, Malenka RC (2006) Synaptic scaling mediated by glial TNF-alpha. *Nature* 440:1054–1059.
17. Ryu EJ, et al. (2008) Analysis of peripheral nerve expression profiles identifies a novel myelin glycoprotein, *MP11*. *J Neurosci* 28:7563–7573.
18. Nagarajan R, Le N, Mahoney H, Araki T, Milbrandt J (2002) Deciphering peripheral nerve myelination by using Schwann cell expression profiling. *Proc Natl Acad Sci USA* 99:8998–9003.
19. Svenningsen AF, Shan WS, Colman DR, Pedraza L (2003) Rapid method for culturing embryonic neuron-glial cell cocultures. *J Neurosci Res* 72:565–573.
20. Tong AH, et al. (2004) Global mapping of the yeast genetic interaction network. *Science* 303:808–813.
21. Phulwani NK, Esen N, Syed MM, Kielian T (2008) TLR2 expression in astrocytes is induced by TNF-alpha- and NF-kappaB-dependent pathways. *J Immunol* 181:3841–3849.
22. Morlon A, Munnich A, Smahi A (2005) TAB2, TRAF6 and TAK1 are involved in NF-kappaB activation induced by the TNF-receptor, Edar and its adaptator Edaradd. *Hum Mol Genet* 14:3751–3757.
23. Barallobre MJ, Pascual M, Del Rio JA, Soriano E (2005) The Netrin family of guidance factors: Emphasis on Netrin-1 signalling. *Brain Res Brain Res Rev* 49:22–47.
24. Paradisi A et al. (2008) NF-kappaB regulates netrin-1 expression and affects the conditional tumor suppressive activity of the netrin-1 receptors. *Gastroenterology* 135:1248–1257.
25. Mattson MP (2003) Insulating axons via NF-kappaB. *Nat Neurosci* 6:105–106.
26. Armstrong SJ, Wiberg M, Terenghi G, Kingham PJ (2008) Laminin activates NF-kappaB in Schwann cells to enhance neurite outgrowth. *Neurosci Lett* 439:42–46.
27. Campana WM (2007) Schwann cells: Activated peripheral glia and their role in neuropathic pain. *Brain Behav Immun* 21:522–527.
28. Hao S, Mata M, Glorioso JC, Fink DJ (2007) Gene transfer to interfere with TNFalpha signaling in neuropathic pain. *Gene Ther* 14:1010–1016.
29. Liu YL, et al. (2007) Tumor necrosis factor-alpha induces long-term potentiation of C-fiber evoked field potentials in spinal dorsal horn in rats with nerve injury: The role of NF-kappa B, JNK and p38 MAPK. *Neuropharmacology* 52:708–715.
30. Zhang Y, et al. (2008) Activation of beta-catenin signaling programs embryonic epidermis to hair follicle fate. *Development* 135:2161–2172.
31. Hiramoto K, Negishi M, Katoh H (2006) Dock4 is regulated by RhoG and promotes Rac-dependent cell migration. *Exp Cell Res* 312:4205–4216.
32. Upadhyay G, et al. (2008) Molecular association between beta-catenin degradation complex and Rac guanine exchange factor DOCK4 is essential for Wnt/beta-catenin signaling. *Oncogene* 27:5845–5855.
33. Hester I, et al. (2007) Transient expression of Nxf, a bHLH-PAS transactivator induced by neuronal preconditioning, confers neuroprotection in cultured cells. *Brain Res* 1135:1–11.
34. Jiang L, Crews ST (2007) Transcriptional specificity of Drosophila dysfusion and the control of tracheal fusion cell gene expression. *J Biol Chem* 282:28659–28668.
35. Takano K, Miki T, Katahira J, Yoneda Y (2007) NXF2 is involved in cytoplasmic mRNA dynamics through interactions with motor proteins. *Nucleic Acids Res* 35:2513–2521.
36. Schafers M, Brinkhoff J, Neukirchen S, Marziniak M, Sommer C (2001) Combined epineurial therapy with neutralizing antibodies to tumor necrosis factor-alpha and interleukin-1 receptor has an additive effect in reducing neuropathic pain in mice. *Neurosci Lett* 310:113–116.
37. Sommer C, et al. (2001) Anti-TNF-neutralizing antibodies reduce pain-related behavior in two different mouse models of painful mononeuropathy. *Brain Res* 913:86–89.
38. Sommer C, Schmidt C, George A (1998) Hyperalgesia in experimental neuropathy is dependent on the TNF receptor 1. *Exp Neurol* 151:138–142.
39. Michailov GV, et al. (2004) Axonal neuregulin-1 regulates myelin sheath thickness. *Science* 304:700–703.
40. Kim GM, et al. (2001) Tumor necrosis factor receptor deletion reduces nuclear factor-kappaB activation, cellular inhibitor of apoptosis protein 2 expression, and functional recovery after traumatic spinal cord injury. *J Neurosci* 21:6617–6625.
41. Paradisi A, et al. (2008) NF-kappaB regulates netrin-1 expression and affects the conditional tumor suppressive activity of the netrin-1 receptors. *Gastroenterology* 135:1248–1257.
42. Chen ZL, Haegeli V, Yu H, Strickland S (2008) Cortical deficiency of laminin gamma1 impairs the AKT/GSK-3beta signaling pathway and leads to defects in neurite outgrowth and neuronal migration. *Dev Biol* 327:158–168.
43. Prestori F, et al. (2008) Altered neuron excitability and synaptic plasticity in the cerebellar granular layer of juvenile prion protein knockout mice with impaired motor control. *J Neurosci* 28:7091–7103.